

## Experiences and expectations of a novel X-ray microsource with focusing mirror. I

A. C. Bloomer\* and U. W. Arndt

MRC Laboratory of Molecular Biology, Hills  
Road, Cambridge CB2 2QH, England

Correspondence e-mail:  
acb1@mrc-lmb.cam.ac.uk

Data are presented from a novel microfocus X-ray generator installed with a choice of ellipsoidal specularly reflecting mirrors. Diffraction data from proteins show the useful flux from this low-power device to be approaching equivalence with that from many far more powerful generators. Intensity measurements show that for small crystals the brilliance is now restricted by the performance of the mirror, which appears to be limited by imperfections in the figure of its surface rather than by a low reflectivity. Suitable choices of ellipsoidal mirror enable the size and divergence of the X-ray beam to be altered readily to match the different requirements of successive samples and appropriate designs are proposed. Alternative types of mirror are expected to be advantageous, especially for the smallest crystals. For crystals of sizes 300  $\mu\text{m}$  or less, which need a small well collimated beam with low divergence, the output from this X-ray tube running at 24 W provides a usable flux similar to that available from rotating-anode generators. The relative performance of this tube and mirror combination becomes increasingly advantageous with the study of ever-smaller crystals.

Received 14 June 1999

Accepted 16 July 1999

### 1. Introduction

This paper reports early experiences with a microfocus X-ray tube made for commercial production based upon the prototype described by Arndt, Long *et al.* (1998) and utilizing the focusing properties of the ellipsoidal mirrors reported by Arndt, Duncumb *et al.* (1998). The prototype tube, which was not operated at power greater than 9 W or 25 kV, used a tungsten-filament emitter within a continuously pumped tube, as distinct from the sealed-tube generator with flat barium dispenser cathode now in production. The aim of the present investigation was to characterize the performance of the first generators of this design manufactured by Bede Scientific Instruments Ltd (Durham, UK) under licence from the MRC, and to assess this against the performance of alternative generators and optical systems now available for laboratory use, making special reference to the requirements for optimum collection of diffraction data from macromolecular crystals. No measurements have previously been reported of the long-term and short-term stability of the combined microfocus tube plus mirror installation.

During the summer of 1998, we received a MicroSource tube (Serial No. 10010 with control unit 40008) on loan for several months from Bede for purposes of evaluation of the performance of this particular implementation of the original design. The 'Medium Ellipsoid' mirror provided (Serial No. ME11.1) had been designed for general utility to produce a balanced compromise between the lowest cross-fire and the

highest intensity. For one week during March 1999, we were loaned a more recent X-ray tube (Serial No. 10024 with control unit 40014) and a 'Small Ellipsoid' mirror (Serial No. SES03-04) made to a different design for reduced cross-fire in the beam.

When the original design parameters of this system were first considered, the required goal was to obtain a focused X-ray beam of suitable dimensions and cross-fire (convergence or divergence) to match crystalline samples with diameters in the range 300–500  $\mu\text{m}$  and mosaic spreads of about 1 mrad. Recent advances elsewhere have led to data collection now mostly utilizing crystals which have been rapidly frozen, a process which often increases their mosaic spread. In consequence, there is now an increased interest in crystals which are very small and those which have a somewhat larger mosaic spread. This has changed the principal requirements for an in-house generator towards requiring a much smaller focused beam but with less stringent restraints upon the acceptable cross-fire. A significant advantage, in theory, of using the collimated beam from a microfocus X-ray tube with adjustable electron focus is the ease with which the beam can be optimized over a varied range of requirements. The choice of parameters is discussed below, together with the constraints which, in practice, limit the simultaneous realization of all goals.

## 2. Experimental arrangement

The early MicroSource tube was installed for use with an image-plate scanner system which is a prototype of the 180 mm MAR scanner, but has in-house designs for collimator, backstop, goniostat and control software. We constructed a tube mounting, enabling alignment of the small lightweight microfocus tube to the much larger (fixed) diffractometer. The initial design of the mounting stand was modified through experience of the stringent demands of maintaining accurate alignment of a 300  $\mu\text{m}$  diameter beam at a distance of up to 1 m from the X-ray source, whose own focal size is only 15  $\mu\text{m}$ .

The more recent tube arrived complete with its own mounting stand and was installed for use with a standard 300 mm MAR scanner, enabling use of the normal slits, ionization chambers and backstop. Fig. 1 shows this arrangement, with the control box being the single module visible below the table-top of one of our safety enclosures. The MicroSource tube, with a Reflex ellipsoidal mirror whose mounting was directly attached to the tube casing, was on a stand which permitted small rotations of the entire assembly about both a horizontal and a vertical axis and also linear translations along horizontal and vertical lines. It was operated at 40 kV and 0.6 mA (power 24 W). The diffractometer could be regarded as if it were fixed.

We have operated the X-ray tube at a power of up to 30 W, with an electron focus of  $15 \times 75 \mu\text{m}$  viewed at a take-off angle of  $12^\circ$  to give a foreshortened isometric beam 15  $\mu\text{m}$  in diameter. In all our stability and flux measurements, we used air-filled ionization chambers, sometimes fitted with a

balanced pair of nickel/cobalt filters (Ross, 1928). Where it was necessary to restrict the measurements to a narrow X-ray wavelength band centred on the Cu  $K\alpha$  line, we used the differences between the response with a nickel  $\beta$ -filter and a balanced cobalt  $\alpha$ -filter. All measurements were performed within the established linear range of the ionization-chamber amplifier. Ionization chamber readings vary by 1–2% in line with changing barometric pressure.

Comparative measurements were made with two rotating-anode X-ray generators, each fitted with a pair of Franks mirrors (Kirkpatrick & Baez, 1948; Franks, 1955). The first was an Elliott GX-13 operated at 40 kV and 60 mA (power 2400 W) equipped with Supper mirrors; the second was a Rigaku RUH3R-HB operated at 50 kV and 100 mA (power 5000 W) equipped with MSC Yale mirrors. Both these rotating-anode generators (RAG) had adjustable mirror systems and the diffractometers were aligned to the focused X-ray beam.

## 3. Present performance

The first comparative intensity measurements on the focused direct beam were reported by Bloomer & Arndt (1998), showing that the flux incident upon a 300  $\mu\text{m}$  diameter sample from the microfocus tube was about 35–40% of that from the GX-13 in our laboratory. Details of that comparison are given in Table 1, which also includes more recent data both from a rotating-anode generator RUH3R-HB newly installed in this laboratory and from the second microfocus tube, which

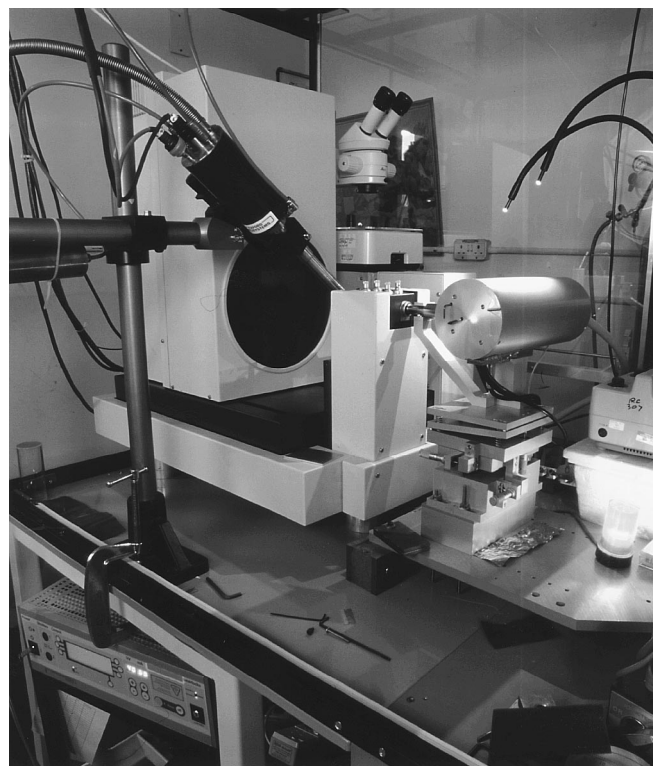


**Figure 1**  
The MicroSource tube installed with a 30 cm MAR scanner.

**Table 1**  
Relative intensity measurements.

Further details of the X-ray generators are given in the text.

(a) Earliest comparison. Intensities are expressed on arbitrary scale,  $I_{LMB}$ , of our ionization chamber. All these measurements are of intensity through a 300  $\mu\text{m}$  diameter sampling aperture at 600 mm from the source.

Source	Focusing mirror(s)	Operating power	MAR slits (mm)	$I_{LMB}$
MicroSource	ME11.1 ellipsoidal mirror	25 W (50 kV, 0.5 mA)	Collimator, 0.3 mm diameter front aperture	0.44
GX-13	Supper 60 mm mirror pair	2400 W (40 kV, 60 mA)	0.2 0.3	0.84 1.21

(b) Recent comparison.  $I_{LMB}$  expressed on the same arbitrary scale and also on scale of internal MAR ionization chamber using chamber 2 (downstream) and a gain of 1. These intensity measurements are without a sampling aperture, but with MAR slit settings.

Source	Focusing mirror(s)	Operating power	MAR slits (mm) (upstream, downstream)	$I_{MAR}$	$I_{LMB}$
MicroSource	SES03-04 ellipsoidal mirror	24 W (40 kV, 0.6 mA)	0.3, 0.2	4.9	1.08
			0.3, 0.3	16.6	1.45
			0.4, 0.4	9.9	2.16
			0.5, 0.5	12.5	2.72
GX-13	Supper 60 mm mirror pair	2400 W (40 kV, 60 mA)	0.2, 0.2	3.6	0.8
			0.3, 0.3	7.4	1.62
RUH3R-HB	Yale/MS mirror pair	5000 W (50 kV, 100 mA)	0.3, 0.3	28.0	6.10

generates at least twice the flux of the earlier tube. These data are also presented on the scale of relative intensities used by the MAR ionization chambers, which will be widely recog-

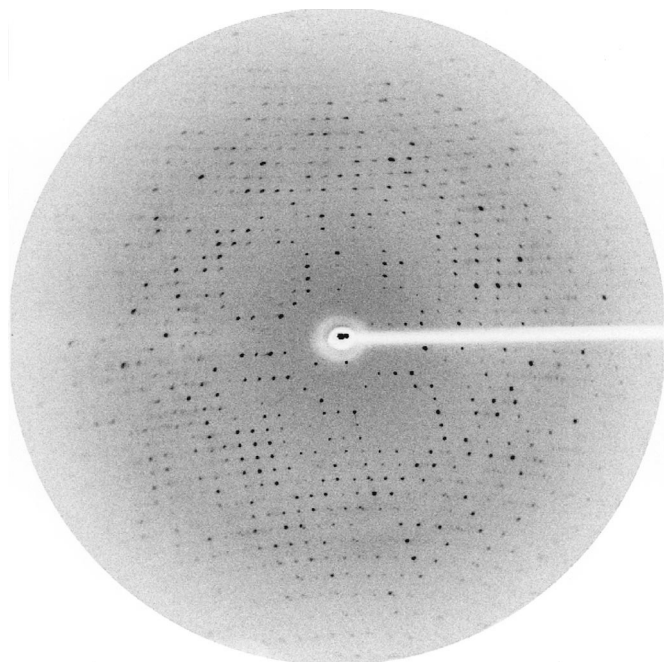


**Figure 2**  
Diffraction pattern from a protein crystal. The image was recorded by a MAR Research 180 mm scanner with an image-plate distance of 128 mm, giving a resolution of 2.6  $\text{\AA}$  at the edge. The oscillation range was  $1.0^\circ$ , the exposure time was 40 min and the crystal used was a frozen crystal of liganded Fab fragment of CAMPATH-1H antibody (James *et al.*, 1999).

nized. The intensities predicted by Arndt, Duncumb *et al.* (1998) based on a power dissipation seven times greater than that in their prototype now appear to have been verified.

A lysozyme crystal was initially mounted on the first MicroSource and then mounted on a GX-13 and diffraction images were obtained under as closely similar conditions as possible, though there were inevitable differences in the collimator aperture or slit settings and in the two beamstops used. When these single images were processed and scaled against standard lysozyme data, the mean intensities were in the ratio of about 1:8, with a better signal-to-noise ratio for the weaker MicroSource data; however, the unavoidable differences between these two data-collection experiments preclude detailed analysis. Complete data sets from proteins were collected and processed satisfactorily, with a typical image being shown in Fig. 2 from a frozen crystal of the Fab fragment of the CAMPATH-1H antibody (James *et al.*, 1999).

Table 2 shows the statistics for three data sets collected in rapid succession from the same crystal of lysozyme; the first was obtained using the early MicroSource, the second with the GX-13 with standard MAR slit settings of 0.3 mm and the third with the GX-13 with the slits narrowed to 0.2 mm. This third data set served as an internal comparison. The same exposure times and detector distances were used throughout. The ratio of mean intensity is about 1:9:4, but the quality indices are broadly similar, indicating that these are not limited by photon statistics. The estimated standard deviations vary far less with resolution for the MicroSource data than for the GX-13 data, and the low-resolution intensities are so different that further investigation is needed. More recent data sets collected with the second MicroSource system with its better focusing mirror suggest that for small lysozyme crystals, the mean diffracted intensity is about 70% of that normally achieved with our GX-13 generators (Gwyndaf Evans, personal communication); the ratio of mean intensity therefore becomes about 6:9:4, even though the mirror in this second system is a small ellipsoid with a lower convergence angle in the beam. The most reasonable explanation for this is that the more recently manufactured tube and mirror deliver improved performance.

Observed differences between the ratio of the diffracted intensities and that of the incident fluxes highlight the need for comparisons to take full account of all parameters. The incident intensity achievable depends on the quality of both the electron focus of the source and the focusing collimators, whereas the diffracted intensity also depends on illuminated volume and other crystal factors. We studied the effect of varying the operating beam current: Table 3 shows the

**Table 2**

Statistics from comparable data sets.

HEWL data collected as 45 or 47 frames, width 1°, distance 120 mm, exposure 3 min, room temperature, data processing from 80 to 2.5 Å. Images were processed by *MOSFLM* (Leslie, 1992) and *DENZO* (Otwinowski & Minor, 1997) and scaled using *SCALA* from the *CCP4* suite of programs (Collaborative Computational Project, Number 4, 1994). Statistics from the image-processing programs are the apparent values of mosaicity and cross-fire as defined by each program. Statistics from *SCALA* include  $\langle\sigma\rangle$ , the observed r.m.s. scatter of observations, and  $\langle sd\rangle$ , the average standard deviation derived from experimental variances after modifying appropriately to obtain a normal distribution of errors. Figures in parentheses and square brackets are those for the outermost and innermost of ten resolution bins, respectively.

X-ray generator	MicroSource	GX-13	GX-13
Operating power	24 W	2400 W	2400 W
Focusing mirror(s)	Ellipsoidal ME11.1	Franks 2 × 6 cm	Franks 2 × 6 cm
MAR slit settings (mm)		0.3, 0.3	0.3, 0.3
Date of data collection	12 Aug 1998	13 Aug 1998	13 Aug 1998
Image numbers	001–045	301–347	501–547
<i>MOSFLM</i>			
‘Mosaicity’	0.24	0.21	0.21
$I/\sigma$	26 (7)	30 (13)	26 (13)
<i>DENZO</i>			
denzo.log	0.20	0.30	0.28
‘cross-fire’			
scalepack.log	0.29	0.24	0.23
‘mosaicity’			
<i>SCALA</i>			
Intensity	1775 (626)	16592 (6261)	8060 (3011)
$\langle I\rangle/\langle\sigma\rangle$ ‘scatter’	[5.6] 5.9 (4.5)	[8.4] 5.4 (4.6)	[5.0] 5.3 (4.7)
$\langle I\rangle/\langle sd\rangle$ ‘signal to noise’	[14.8] 10.9 (5.9)	[8.9] 11.0 (8.7)	[8.3] 10.6 (8.0)
Multiplicity	3.1 (3.0)	3.3 (3.4)	3.3 (3.4)
PCV (%)	12.4 (20.4)	13.0 (18.3)	13.2 (18.5)
$R_{\text{sym}}$ (%)	9.0 (15.3)	9.7 (12.9)	9.9 (13.5)

increases in incident intensity per unit area which were observed with decreasing sample diameters; these do not change as the current increases from 0.1 to 0.5 mA. This confirms that the apparent size of the electron focus on these tubes does not increase with beam current over the range 0.1–0.5 mA studied here; the relative advantages of a micro-focus source for smaller crystals should therefore be maintained if increased power loadings on the electron target become achievable. Simulations have suggested (Arndt, Long *et al.*, 1998) that if it were possible to increase the tube current beyond this range, the use of an immersion objective as the magnetic focusing lens of the X-ray tube may become necessary in order to preserve a small electron focus.

#### 4. X-ray tube stability

The short-term X-ray stability is excellent once the tube has reached thermal equilibrium. Very great care was necessary in the design and construction both of the adjustable mirror mounts which are attached to the tube and are used to move the mirror with respect to the tube focus and of the adjustments which align the tube–mirror assembly with respect to the crystal. For a stringent test, we have monitored the intensity passing through a sample aperture of 300 µm over periods of many hours.

**Table 3**

Size of focal spot does not increase with current up to 0.5 mA.

Incident intensity through a sampling aperture of given diameter was measured for the MicroSource tube operating at 48 kV with both 0.1 and 0.5 mA beam currents. These measurements were made with the early MicroSource tube and mirror ME11.1, but there is no reason to suspect that this relationship between beam current and focused flux will differ between different tubes.

Diameter of aperture at sample position <i>D</i> (mm)	1.0	0.7	0.5	0.3
Current 0.5 mA, operating power 24.0 W				
Total intensity, <i>I</i> , as recorded for each aperture	1.45	0.88	0.48	0.24
Repeated to check reproducibility of sample-aperture positioning	1.45	0.88	0.53	0.25
Intensity per unit area of sample, $I_5 = I/D^2$	1.45	1.80	2.02	2.76
Relative intensity per unit area	1.00	1.24	1.39	1.90
Current 0.1 mA, operating power 4.8 W				
Total intensity, <i>I</i> , as recorded for each aperture	0.26	0.16	0.09	0.05
Intensity per unit area of sample, $I_1 = I/D^2$	0.26	0.33	0.36	0.51
Relative intensity per unit area	1.00	1.27	1.38	1.94
Ratio of intensity at high current to low, $I_5/I_1$	5.51	5.37	5.54	5.33

With the second tube, which was operating at 24 W (40 kV, 0.6 mA), we observed no drop in output intensity over the entire one-week period available for observation. With the earlier first tube, whose output was always three or more times less intense than that of the later tube, we observed no drop in output intensity during a period of more than one week when the operating power was less than 18 W. When the power was between 18 and 25 W, its measured intensity fell by up to 20% in the first 24 h but then remained constant. Only when the power exceeded 25 W did we suspect some target damage, and even then the target was not pierced and the initial intensity was regained after we applied a slight deflection of the electron focus onto a different area on the surface of the target. Aspects of this time-dependent decrease remain to be fully understood, but its exact course appears to be determined by the initial smoothness of the target surface, according to the following considerations.

We shall assume that the target is covered with a roughened copper layer which has a linear absorption coefficient,  $\mu$ , of 75% of that of bulk copper and is thus equal to  $0.035 \mu\text{m}^{-1}$ . This layer has no effect other than that of attenuating the X-rays generated at some depth *z* within the target. The initial thickness of this roughened layer may be taken as somewhere between 0.4 and 3 µm. In engineering practice, surfaces with these peak-to-peak roughnesses are referred to as having a ‘mirror finish’ and a ‘smooth finish’. (To give an adequate reflectivity, an X-ray mirror surface must be much smoother than an optical mirror surface and needs to have an r.m.s. peak-to-peak roughness of less than 20 Å.) The effect of the choice of take-off angle,  $\varphi$ , is shown in Fig. 3, from which it is seen that the intensity *I* emerging at angle  $\varphi$  through a layer of thickness *z* is  $I = I_0 \exp[-(\mu z/\sin\varphi)]$ , where  $I_0$  is the intensity generated. Thus, it is seen that  $dI/dz = -I_0(\mu/\sin\varphi) \times \exp[-(\mu z/\sin\varphi)]$  and hence  $dI/I = -dz(\mu/\sin\varphi)$ .

Therefore,  $dI/I$  lies between 6.7 and 50% for a 12° take-off angle, but only between 2 and 15% for a 45° take-off angle. This model and the estimates suggested by it for the intensity reduction make no claim to any precision, but they do illus-

trate both the importance of ensuring the smoothest possible target surface and also the greater latitude in quality of surface finish allowed with a larger take-off angle.

It is well known that the output of X-ray tubes can decrease by up to 50% during the first few hours of target life, almost certainly as a result of the roughening of the surface. Source uniformity owing to target roughness has been discussed by Wyckoff & Agard (1977). The exact cause of this roughening when the hot spot has remained well below the melting point of copper is not known. The time required to evaporate a 0.1  $\mu\text{m}$  thick layer of copper is  $5.6 \times 10^{10}$  h at 800 K and is still  $2.4 \times 10^6$  h at 1000 K; the cause of surface damage is therefore not a simple thermal one.

### 5. Lifetime of X-ray tube and mirrors

The earlier tests reported (Arndt, Duncumb *et al.*, 1998; Arndt, Long *et al.*, 1998) were carried out on a tube equipped with a tungsten filament instead of the present barium dispenser cathode, and these filaments had unacceptably short lifetimes. Our present tubes are very much better: we have already operated the first tube for over 5000 h (7 months), usually at its full power of 24 W, without observing a decrease of cathode emission onto the electron target.

The specific power loading at the upstream end of a mirror positioned at  $x_1 = 11$  mm from the target of a MicroSource operated at 24 W is less than that of a mirror positioned at  $x_1 = 80$  mm from the target of a rotating-anode generator operated at 4000 W by a factor of  $(4000/24) \times (11/80)^2 \simeq 3.15$ . Consequently, one would expect the mirror to last 3.15 times longer in the MicroSource beam as compared with the mirrors used in a rotating-anode generator.

### 6. Insertion gain

A quantity which is easy to determine for any focusing element is the 'insertion gain'. For this measurement, a small aperture is placed at the focus of the mirror and the intensity of the X-rays passing through this aperture is recorded both with the mirror in position and with the mirror removed. The insertion gain is the ratio of these two intensities. The gain thus defined is not a single quantity but is a function of the aperture size. We have mounted a series of apertures of different diameters on the spindle axis of our goniometer and brought each in turn into the X-ray beam. The beam was not restricted

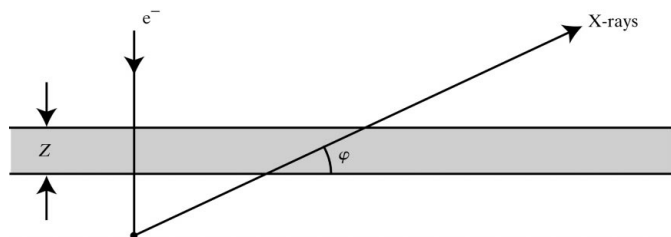


**Figure 3**  
The influence of the take-off angle on absorption by the target of the X-rays generated within it.

by any other aperture smaller than at least twice the diameter of our largest sampling aperture.

In calculating the theoretical performance of a mirror with a microfocus X-ray tube, one may make two assumptions: (i) that the mirror forms a true image of the X-ray source at its focus with a predictable magnification and (ii) that the reflectivity of the mirror surface expressed as a function of the angle of incidence can be calculated on the basis of Fresnel's formula modified by a reasonable estimate of the surface roughness of the mirror. We show here that the calculated insertion gain of our mirrors derived in this way is up to 30 times greater than the observed value. In attempting to improve the performance of the mirrors and even in deciding which type of mirror to use, it is important to know where the above assumptions break down.

### 7. Ellipsoidal mirrors

The characteristics of ellipsoidal mirrors can be tailored according to the particular diffraction problem under investigation by a suitable choice of the mirror parameters (Fig. 4). These are:  $2a$ , the major axis of the ellipsoid;  $x_1$  and  $x_2$ , the distances from the source of the upstream and downstream ends of the mirror;  $y_1$  and  $y_2$ , the radii of the ellipsoid at positions  $x_1$  and  $x_2$ .

The largest angle of incidence on the reflecting surface of the mirror occurs at its upstream end, where it is chosen to be equal to  $\theta_c$ , the critical angle for total external reflection at the given wavelength. The radii of the ellipsoid are therefore given by

$$y_1 = 2\theta_c x_1 (2a - x_1) / 2a,$$

$$y_2 = y_1 [(x_2/x_1)(2a - x_2)/(2a - x_1)]^{1/2}.$$

The crossfire,  $2\gamma$  (the angle between extreme rays striking the specimen at the mirror focus), is determined by the angle subtended at this focus by the exit pupil of the mirror and is therefore given by

$$2\gamma = 2y_2 / (2a - x_2).$$

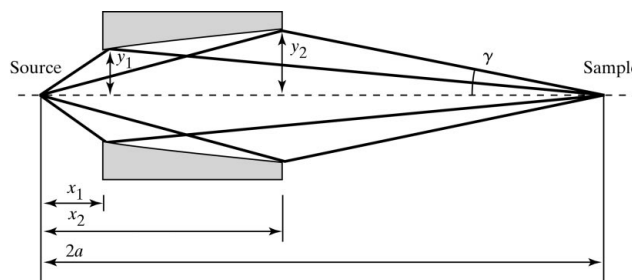


**Figure 4**  
The form of the elliptical mirror. The major axis  $2a$  may be in the range 75–1500 mm, whereas the exit aperture  $2y_2$  lies in the region 0.4–2.4 mm. The angle  $2\gamma$  determines the cross-fire on the sample and is in the range 1.5–10 mrad (0.09–0.6°).

**Table 4**  
Parameters of ellipsoidal mirrors.

The calculated crossfire  $2\gamma$ , solid angle of collection  $\Omega$ , upstream and downstream radii  $y_1$  and  $y_2$ , respectively, and the smallest magnification  $M_2$  are shown for a source of diameter of 15 mm with mirror of length 20 mm placed at varying distances,  $x_1$ , from the source with highest magnification,  $M_1$ , appropriate for crystal sample sizes ranging from 150 to 450 mm. Calculations are for gold mirrors for which the critical angle is 9.96 mrad for Cu  $K\alpha$  wavelength.

$x_1$ (mm)	10	20	30	40	50
$x_2$ (mm)	30	40	50	60	70
Sample diameter 450 mm, $M_1 = 30$					
$2a$ (mm)	310	620	930	1240	1550
$y_1$ (mm)	0.193	0.386	0.578	0.771	0.964
$y_2$ (mm)	0.323	0.536	0.738	0.936	1.133
$M_2$	9.33	14.50	17.60	19.67	21.14
$2\gamma$ (mrad)	2.30	1.85	1.68	1.59	1.53
$\Omega$ (msterad)	0.804	0.603	0.483	0.402	0.345
Sample diameter 300 mm, $M_1 = 20$					
$2a$ (mm)	210	420	630	840	1050
$y_1$ (mm)	0.190	0.379	0.569	0.759	0.949
$y_2$ (mm)	0.312	0.523	0.722	0.918	1.111
$M_2$	6.00	9.50	11.60	13.00	14.00
$2\gamma$ (mrad)	3.46	2.75	2.49	2.35	2.27
$\Omega$ (msterad)	0.791	0.594	0.475	0.396	0.339
Sample diameter 200 mm, $M_1 = 13.33$					
$2a$ (mm)	143.3	286.6	429.9	573.2	716.5
$y_1$ (mm)	0.185	0.371	0.556	0.741	0.926
$y_2$ (mm)	0.296	0.504	0.699	0.891	1.080
$M_2$	3.78	6.17	7.60	8.55	9.24
$2\gamma$ (mrad)	5.22	4.09	3.68	3.47	3.34
$\Omega$ (msterad)	0.773	0.580	0.464	0.387	0.331
Sample diameter 150 mm, $M_1 = 10$					
$2a$ (mm)	110	220	330	440	550
$y_1$ (mm)	0.181	0.362	0.543	0.724	0.905
$y_2$ (mm)	0.281	0.486	0.678	0.865	1.050
$M_2$	2.67	4.50	5.60	6.33	6.86
$2\gamma$ (mrad)	7.01	5.40	4.84	4.55	4.37
$\Omega$ (msterad)	0.756	0.567	0.453	0.378	0.324
Sample diameter 100 mm, $M_1 = 6.67$					
$2a$ (mm)	77	153	230	307	383
$y_1$ (mm)	0.173	0.346	0.520	0.693	0.866
$y_2$ (mm)	0.251	0.452	0.636	0.816	0.994
$M_2$	1.56	2.83	3.60	4.11	4.48
$2\gamma$ (mrad)	10.76	7.97	7.07	6.62	6.34
$\Omega$ (msterad)	0.723	0.542	0.434	0.361	0.310

A low crossfire, therefore, requires a long mirror-to-crystal distance and/or small-radius ellipsoid which, in turn, necessitates a short mirror-to-source distance.

The solid angle subtended by the mirror at the source,  $\Omega$ , determines the fraction of the generated X-rays which is collected by the mirror. This angle is given by

$$\Omega = \pi[(y_1/x_1)^2 - (y_2/x_2)^2],$$

$$\Omega = 4\pi\theta_c^2[(x_2 - x_1)/x_2][(2a - x_1)/2a],$$

such that the highest collectable intensity requires a short distance from mirror to source and/or a long ellipsoid of large radius.

X-rays reflected by a point on the mirror are ‘magnified’ by the ratio of the distances of that point from the image and from the source, where the magnification is the ratio of the diameter of the focused image to that of the original X-ray source. The two extreme values,  $M_1$  and  $M_2$ , the magnifications

at the entrance and exit pupils of the mirror at  $x_1$  and  $x_2$ , respectively, are

$$M_1 = (2a - x_1)/x_1,$$

$$M_2 = (2a - x_2)/x_2.$$

For a typical ellipsoid,  $M_2$  is always smaller than  $M_1$  by a factor in the range 1.5 to 3 or 4. This variation of magnification along the length of the mirror means that these glancing-incidence ellipsoidal mirrors cannot form a true image at the ‘focus’ for a non-zero source size and therefore suffer from extreme coma aberration (Wolter, 1952). However, the images formed by downstream elements of the mirror will always fall inside the diameter of the image produced by the upstream part of the mirror, so that all the focused beam diameters calculated here on the basis of  $M_1$  give an upper limit to the focal size [whereas the magnifications used by Arndt and co-workers (Arndt, Duncunb *et al.*, 1998; Arndt, Long *et al.*, 1998) were the geometric mean of  $M_1$  and  $M_2$ ].

From Liouville’s theorem, it follows that the ratio of the angle of collection of rays into a focusing element to the angle of cross-fire of the rays emerging from it is equal to the magnification produced by that element, which is the ratio of the distances from the element to the focused image and to the source. This constraint prevents the mirror parameters from all being simultaneously optimized and necessitates either a compromise design or the use of a variety of different mirrors for different purposes.

Table 4 shows mirror parameters calculated for different values of  $x_1$  and  $2a$  chosen to give different focused X-ray beam diameters at the sample. The length of the mirror,  $x_2 - x_1$ , has been kept constant throughout at 20 mm. The greatest efficiency in diffraction data collection results when the beam diameter is equal to the sample diameter; thus, the magnification  $M_1$  has been varied keeping the source size fixed at its present value of 15  $\mu\text{m}$ . The overall distance from source to sample,  $2a$ , being the major axis of the ellipsoid, is wholly determined by the choices made for  $x_1$  and  $M_1$ . It will be seen from the table that, especially for a small beam diameter, a large value of  $\Omega$  necessarily results in a large crossfire  $2\gamma$  and requires a short distance  $x_1$ . Low crossfire requires a long distance  $x_1$  and higher values of magnification  $M_1$ . In practice, it is not always possible to achieve the exact design value of  $2a$ , the major axis of the ellipsoidal mirror, owing to manufacturing errors in the surface figuring. The difficulty of producing toroidal mirrors increases as the diameter decreases. It is this fact which sets a practical lower limit to  $y_1$  and thus to  $x_1$ .

It should be noted that a more favourable compromise between the requirements to make both the crossfire and the beam size at the sample small is possible if the source size were smaller than 15  $\mu\text{m}$ . This can be achieved by stronger focusing of the electron beam (Arndt, Long *et al.*, 1998), which is only possible with a shorter focal length lens (an immersion objective), since use of an aperture in the X-ray tube would probably just reduce the tails of the electron distribution in the focus.

**Table 5**

Observed and calculated insertion gains.

The gains measured for the small ellipsoid (low cross-fire) mirror SES03-4 are compared with those calculated for values of r.m.s. surface roughness  $\sigma$  with corresponding mean reflectivity  $\bar{R}$  and with a sampling aperture at a distance of 300 mm from the source.

Diameter of sampling aperture (mm)	1.0	0.7	0.5	0.3	0.25	0.2	0.15
Measured flux through aperture (% of incident)	15	11	8	4	nd	nd	1.5
Observed gain, $G_{\text{obs}}$ (measured or extrapolated from Fig. 7)	20	29	39	60	70	85	110
Calculated gain, $G_{\text{calc}}$							
$\sigma = 10 \text{ \AA}$ , $\bar{R} = 0.25$	24	50	90	260	370	580	1030
$\sigma = 5 \text{ \AA}$ , $\bar{R} = 0.8$	75	150	300	820	1180	1850	3280
Ratio $G_{\text{calc}}/G_{\text{obs}}$							
$\sigma = 10 \text{ \AA}$ ,	1.2	1.7	2.3	4.3	5.3	6.8	9.4
$\sigma = 5 \text{ \AA}$	3.8	5.2	7.7	14	17	22	30

Fig. 5 shows the measured diameter of the focused beam from an ellipsoidal mirror (ME11.1) as a function of distance from the X-ray source. There are two curves corresponding to two slightly different adjustments of  $x_1$ , the distance of the mirror from the source. This mirror was designed to have a major axis of 600 mm and all of our measurements were made at this distance. The minimum beam diameter should occur at 600 mm distance, but the departure from the design parameters was such that the smallest beam was achieved at about 450 mm, which can be regarded as a 'false-focus' position. Other mirrors have behaved in a similar way, although some have come close to the design performance (John Wall, personal communication). The variation in diameter of the X-ray beam reflected from an ellipsoidal mirror has been illustrated elsewhere (Fig. 9 in Arndt, Duncumb *et al.*, 1998), but a particularly clear view of the beam from mirror ME11.1 at a distance of 350 mm from the source, as recorded by a high-gain X-ray imager (XRI), is shown here in Fig. 6, which distinguishes the annular focused beam and the central unfocused beam. All of our reported measurements with the second mirror (SES03-4) were made at an identified 'false-focus' position, with a source-to-sample distance of 300 mm, whereas the design value was the same as that for ME11.1 with a focal distance of 600 mm.

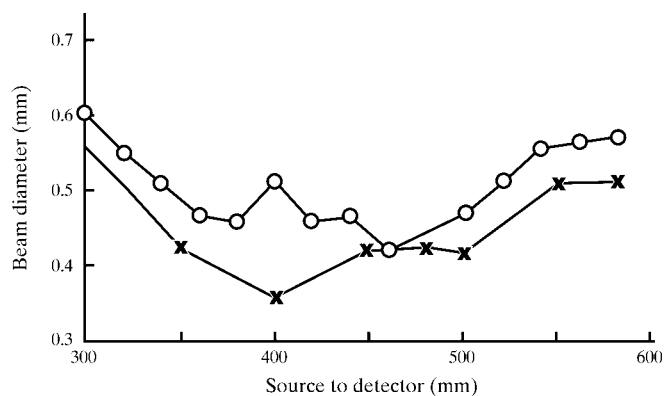


**Figure 5**

Measured diameter of the focused beam from an ellipsoidal mirror (ME11.1) as a function of distance from the X-ray source. The two curves correspond to two slightly different adjustments of  $x_1$ , the distance of the mirror from the source.

The focusing ability of the present mirrors can be assessed by measurement of the insertion gain. With the measuring system already described, we have measured the insertion gain as a function of sample-aperture diameter for an ellipsoidal mirror (SES03-4) recently manufactured by Reflex SRO (Prague). The results shown in Fig. 7 demonstrate that the advantage of a focused beam over a pin-hole collimated beam increases for small-diameter samples, even for mirrors which are still far from perfect.

Even our best mirrors still fall far short of reaching their theoretical insertion gain. This can be calculated from the solid angles subtended at the source by the mirror and by the pinhole and from the mean reflectivity of the mirror,  $\bar{R}$ , which depends upon  $\sigma$ , the r.m.s. surface roughness of the mirror. Table 5 gives the insertion gains calculated for the values of  $\sigma$  and  $\bar{R}$  and the measured values for mirror SES03-4. It is clear that one can expect considerably increased gains as the mirrors are further improved.

Between the first and second mirrors which we studied, there was an approximate doubling in the number of photons focused into our sampling apertures of 0.15 and 0.3 mm, even though the second mirror was a small ellipsoid designed to give a smaller convergence angle at the crystal. This suggests that the techniques for manufacture of these mirrors are being developed rapidly, with immediate and obvious benefits.

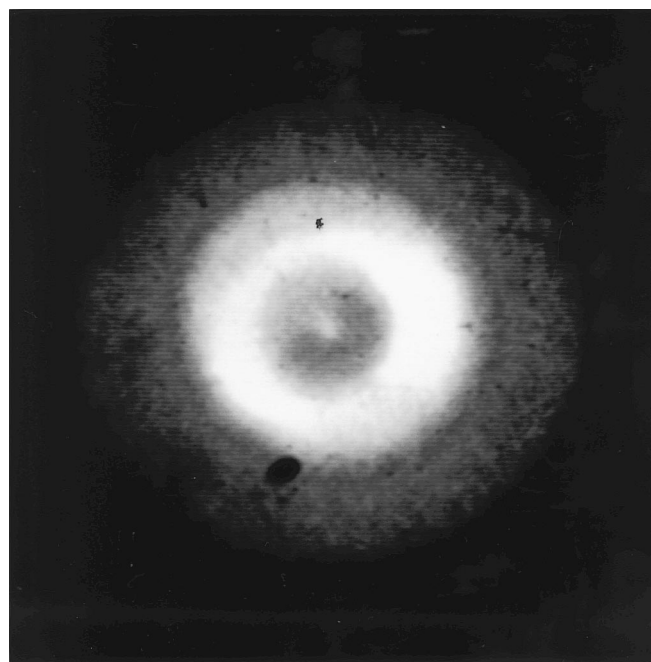


**Figure 6**

Beam reflected by mirror ME11.1 at a distance of 350 mm from the source. The picture was recorded by a high-gain X-ray imager (XRI). Black spots are blemishes on the face of the XRI. The central part of the image would not be visible with a low-gain XRI.

It should be noted that the comparisons of the X-ray intensity with and without the mirror were carried out with the sampling aperture at 300 mm from the source. This gives a somewhat more realistic comparison than the measurements presented earlier (Arndt, Duncumb *et al.*, 1998; Arndt, Long *et al.*, 1998) at 600 mm. Fig. 5 shows that the diameter of the reflected beam at these two distance are not very different; the solid angle subtended by the aperture *without* a mirror, of course, varies with the inverse square of the distance.

We have also measured the ratio of the X-ray flux through various apertures at the mirror focus to the flux falling on the mirror (SES03-04). We used sample apertures in the range

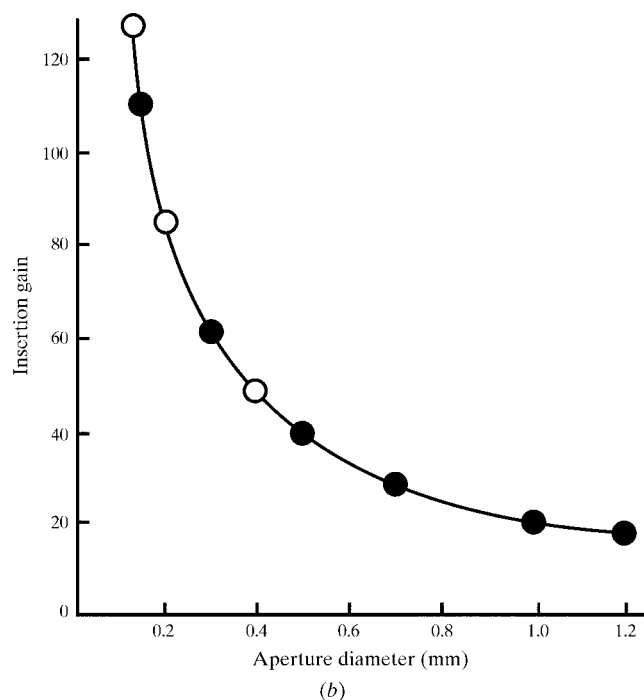
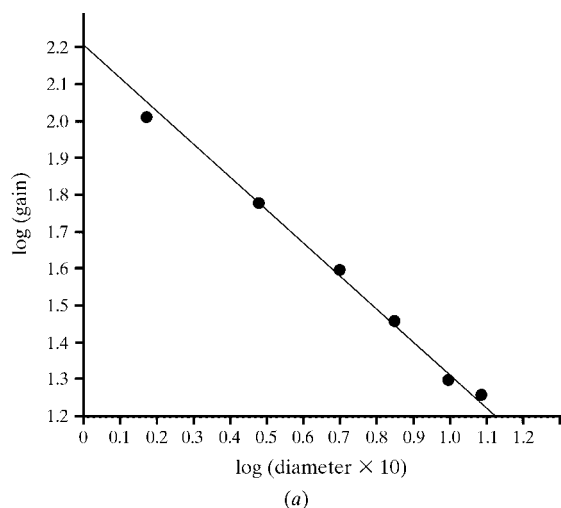


**Figure 7** Measured insertion gain for mirror SES03-4 as a function of aperture diameter. Filled circles represent measured data points, empty circles represent data points obtained by extrapolation. (a) shows a linear relationship between log (gain) and log (diameter) and (b) shows the high insertion gains which can be expected for smaller sample diameters.

0.15–1.2 mm. Fig. 8 shows this ratio as a function of the aperture diameter and also the expected ratio of reflected to incident X-ray flux calculated for a range of mean reflectivities on the assumption that a fraction  $\bar{R}$  of the incident X-rays reaches the focus. These horizontal lines should thus be reached asymptotically by the experimental curves at a focus of diameter  $M$  times the diameter of the source. For this particular mirror with magnification  $M_1$  equal to 26.67, this should be reached at 0.4 mm for a source size of 15  $\mu\text{m}$ . The mean reflectivity is very unlikely to be as small as 0.2, which would correspond to an r.m.s. surface roughness of about 17  $\text{\AA}$ . Therefore, most of the intensity losses can be attributed to aberrations in the mirror figure which result in X-rays being reflected well outside the geometrical focus. This argument can be used to show where and how the mirrors can be improved.

Separate experiments have established that the fore-shortened source size of the X-ray tube (full width at 10% of maximum) is about 15  $\mu\text{m}$ . The magnification of the mirror SES03-4, that is the ratio of the image to the object distance, is between 23 at the upstream end and 7.0 at the downstream end. This variation means the mirror cannot form a good image of this source. However, one might expect that all the reflected rays will pass through an aperture of diameter  $23 \times 15 = 345 \mu\text{m}$  and that the intensity through apertures larger than this would not be greater. Our measurements presented in Fig. 8 show that the recorded intensity continues to increase with aperture diameter up to the limit of our measurements (which do not extend beyond 1.0 mm because there are other beam-limiting constrictions further upstream). Coma, therefore, is not the only cause of image broadening.

It can be seen from Fig. 8 that only 4 and 1.5% of the intensity incident upon this mirror are focused into sample

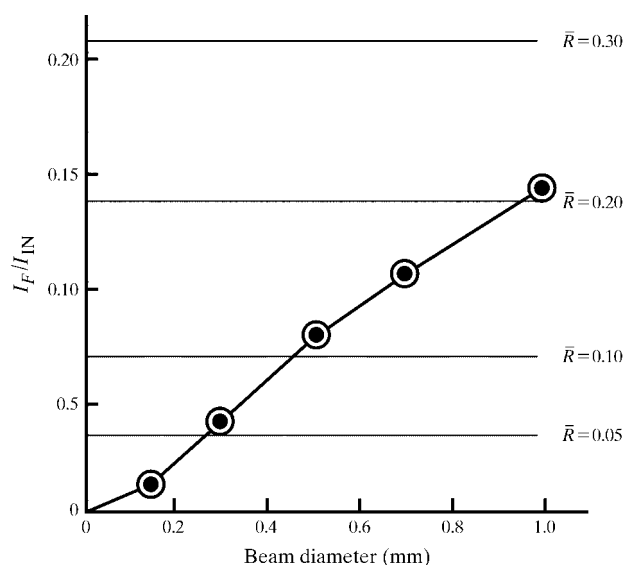


**Figure 8** Measured ratio of reflected to incident X-ray flux and calculated values. Observed values of the ratio are plotted as a function of the sampling-aperture diameter and also the expected ratio of reflected to incident X-ray flux calculated for a range of mean reflectivities.

apertures of 300 mm and 150 mm diameter, respectively; therefore, there is scope for improvement by factors of 25 and 60, respectively, in the focusing for small crystals.

We have used the measurements of X-ray intensity through the series of apertures without the mirror being in position to determine  $I_O$ , the intensity per unit solid angle emitted by the X-ray tube. From the known dimensions of the mirror we could calculate  $\Omega_1$  and  $\Omega_2$ , the solid angles subtended at the source by the entrance and exit pupils of the mirror, respectively, and thus the intensity incident on the mirror,  $I_{IN}$ , where  $I_{IN} = I_O(\Omega_1 - \Omega_2)$ . In Fig. 8, we show the ratio  $I_F/I_{IN}$ , where  $I_F$  is the focused intensity through the apertures with the mirror in position. If the image produced by the mirror were perfect and had a diameter of  $\sim 200 \mu\text{m}$ , then for aperture diameters larger than  $\sim 200 \mu\text{m}$  we should be able to write  $I_F = I_{IN}\bar{R}$ , where  $\bar{R}$  is the mean reflectivity of the mirror surface averaged over all angles of incidence on the mirror.

We have determined the reflectivity  $\bar{R}$  in the following way. We measured  $I_M$ , the total radiation at the immediate exit of the mirror.

$$\begin{aligned} I_M &= \text{radiation reflected by mirror} \\ &\quad + \text{radiation not striking mirror} \\ &= I_{IN}\bar{R} + I_O\Omega_2 \\ &= I_O[\bar{R}(\Omega_1 - \Omega_2) + \Omega_2], \end{aligned}$$

so that

$$\bar{R} = [(I_M/I_O) - \Omega_2]/(\Omega_1 - \Omega_2).$$

We found  $\bar{R} = 0.53$ . This value is high, because  $I_M$  includes radiation scattered by the mirror as well as geometrically reflected X-rays. Nevertheless, this result seems to indicate that the low experimental value of  $I_F/I_{IN}$  is a consequence of imperfections in the figure of the mirror rather than of a low reflectivity. This is a hopeful conclusion, in that improvements in the long-range perfection of the mirror surface can be expected to produce large increases in the intensity of the focused X-ray beam.

## 8. Conclusions

The performance of the MicroSource system as studied here has been shown to be equivalent to that of many laboratory

rotating-anode generators, though it does not yet surpass the most powerful of the latest modern high-powered tubes with focusing monochromators. The first ellipsoidal mirrors have achieved significant focusing which appears to be limited by the precision of the surface figuring rather than its reflectivity. This indicates that considerable improvements in the mirrors can be expected. It is already clear, however, that the combination of its present performance and future promise with the flexibility of its modular design, which allows easy interchange between mirrors, and with its energy-saving minimal maintenance, enabling greatly reduced need for cooling water and electricity, will ensure that this tube has a central role within many laboratories where state of the art diffraction data are collected from macromolecular crystals.

We gratefully acknowledge loan from Bede Scientific Instruments Ltd (Durham, UK) of two X-ray tubes and mirrors as studied here and assistance in setting them up from J. Wall and M. Taylor. We thank colleagues for useful discussions and for assistance with data collection, especially G. Evans, L. C. James, A. J. McCoy and D. J. Owen. MicroSource is a trade mark of Bede Scientific Instruments Ltd.

## References

- Arndt, U. W., Duncumb, P., Long, J. V. P., Pina, L. & Inneman, A. (1998). *J. Appl. Cryst.* **31**, 733–741.
- Arndt, U. W., Long, J. V. P. & Duncumb, P. (1998). *J. Appl. Cryst.* **31**, 936–944.
- Bloomer, A. C. & Arndt, U. W. (1998). *CCP4 Newsllett.* **35**, 43–45.
- Collaborative Computational Project, Number 4 (1994). *Acta Cryst.* **D50**, 760–763.
- Franks, A. (1955). *Proc. Phys. Soc. London B*, **68**, 1054–1069.
- James, L. C., Hale, G., Waldmann, H. & Bloomer, A. C. (1999). *J. Mol. Biol.* **289**, 293–301.
- Kirkpatrick, P. & Baez, A. V. (1948). *J. Opt. Soc. Am.* **38**, 766–744.
- Leslie, A. G. W. (1992). *Jnt CCP4/ESF-EACMB Newsllett. Protein Crystallogr.* **26**.
- Otwinowski, Z. & Minor, W. (1997). *Methods Enzymol.* **276**, 307–326.
- Ross, P. A. (1928). *J. Opt. Soc. Am.* **16**, 433–438.
- Wolter, H. (1952). *Opt. Röntgenstr. Ann. Phys. (Leipzig)*, **10**, 94–113.
- Wyckoff, H. W. & Agard, D. (1977). *The Rotation Method In Crystallography*, edited by U. W. Arndt & A. J. Wonacott, ch. 13, pp. 187–206. Amsterdam: North-Holland.